Supporting Information

Upraising the O 2p orbital by integrating Ni with MoO_2 for accelerating hydrogen evolution kinetics

Xiong Liu,[†,#] Kun Ni,[‡,#] Chaojiang Niu,[†,#] Ruiting Guo,[†] Wei Xi,[*,§] Zhaoyang Wang,[†] Jiashen Meng,[†] Jiantao Li,[†] Yanwu Zhu,[‡] Peijie Wu,[†] Qi Li,[†] Jun Luo,[§] Xiaojun Wu,[*,‡] and Liqiang Mai[*,†]

[†]State Key Laboratory of Advanced Technology for Materials Synthesis and Processing, Wuhan University of Technology, Wuhan 430070, China

[‡]Hefei National Laboratory for Physical Sciences at the Microscale, School of Chemistry and Materials Sciences, CAS Key Laboratory of Materials for Energy Conversion, CAS Center for Excellence in Nanoscience, iChEM (Collaborative Innovation Center of Chemistry for Energy Materials), University of Science and Technology of China, Hefei, Anhui 230026, China

[§]Center for Electron Microscopy and Tianjin Key Laboratory of Advanced Functional Porous Materials, Institute for New Energy Materials & Low-Carbon Technologies, School of Materials Science and Engineering, Tianjin University of Technology, Tianjin 300384, China

Corresponding Authors

[*]mlq518@whut.edu.cn

[*]xjwu@ustc.edu.cn

[*]weiandna1234@163.com

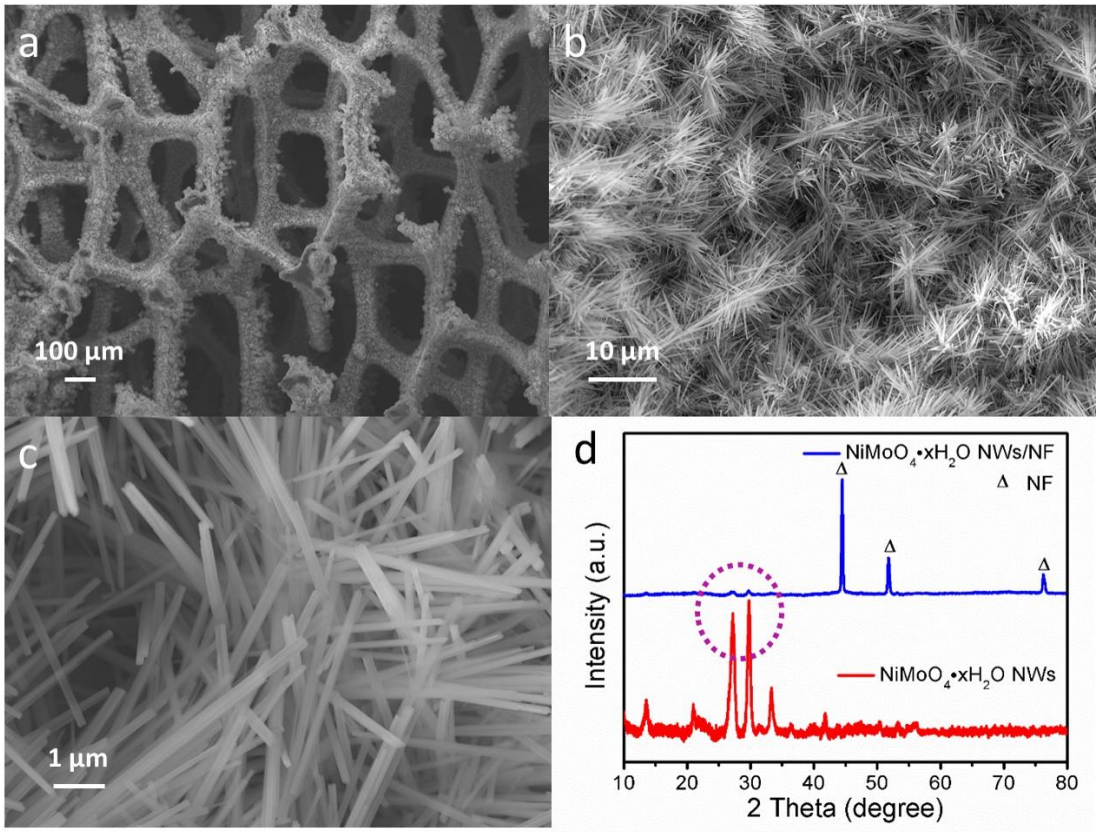

Figure S1. (a-c) SEM images of $NiMoO_4 \cdot xH_2O$ nanowires grown on the nickel foam ($NiMoO_4 \cdot xH_2O$ NWs/NF). (d) XRD patterns of $NiMoO_4 \cdot xH_2O$ NWs and $NiMoO_4 \cdot xH_2O$ NWs/NF.

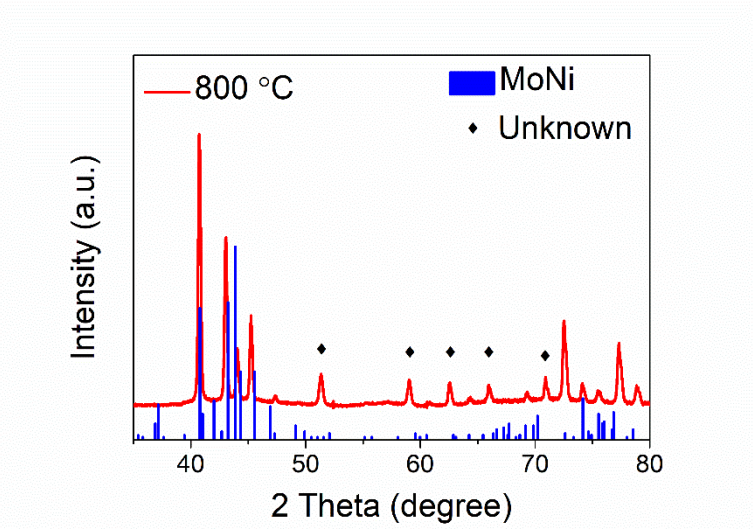

Figure S2. XRD pattern of $NiMoO_4 \cdot xH_2O$ NWs calcined at 800 °C in Ar/H_2.

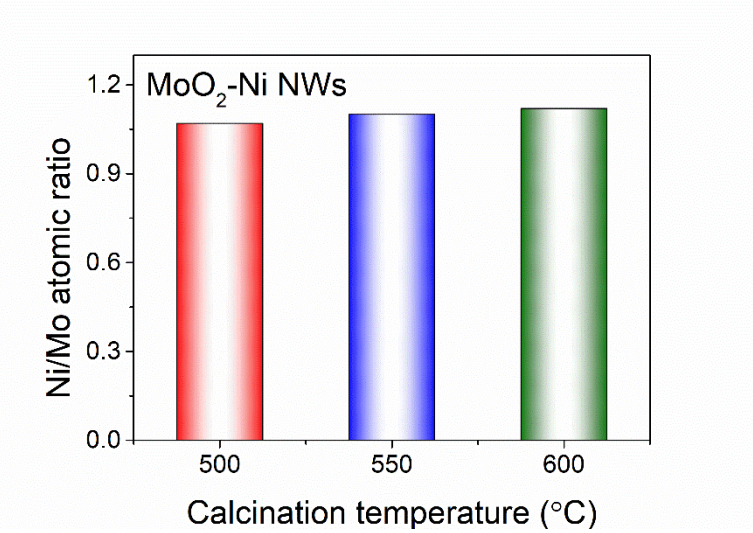

Figure S3. ICP results of MoO_2-Ni-x (x = 500, 550 and 600) NWs, respectively.

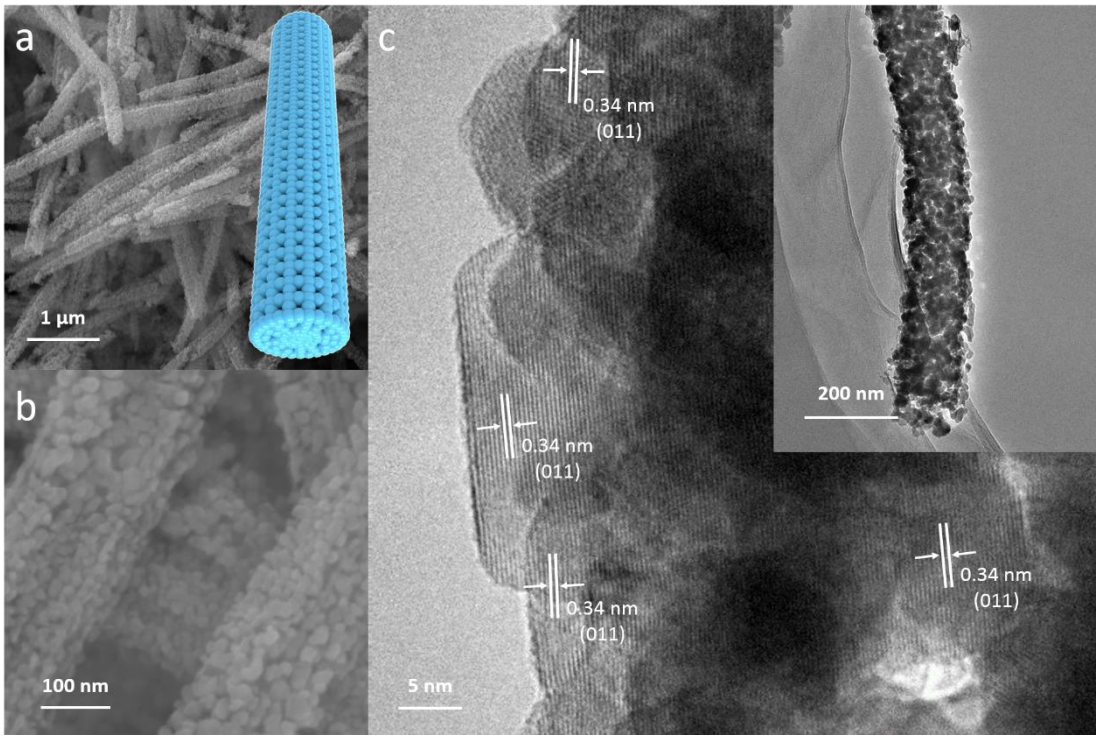

Figure S4. (a, b) SEM and (c) HRTEM images of mesoporous MoO_2 nanowires. The inset in (c) is the TEM image of mesoporous MoO_2 nanowires.

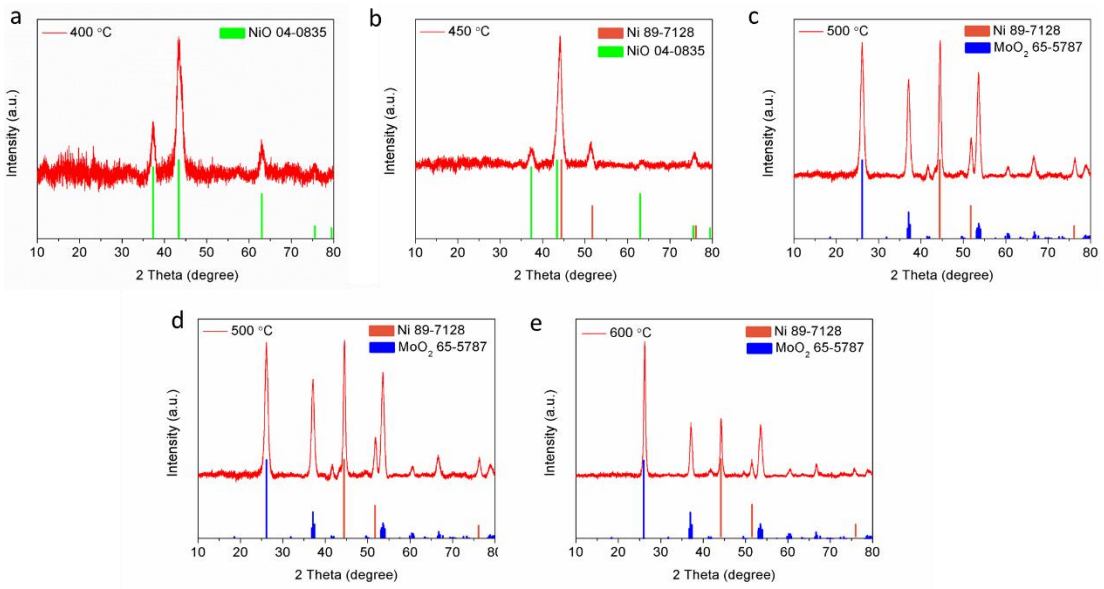

Figure S5. XRD patterns of $NiMoO_4 \cdot xH_2O$ NWs calcined at different temperatures.

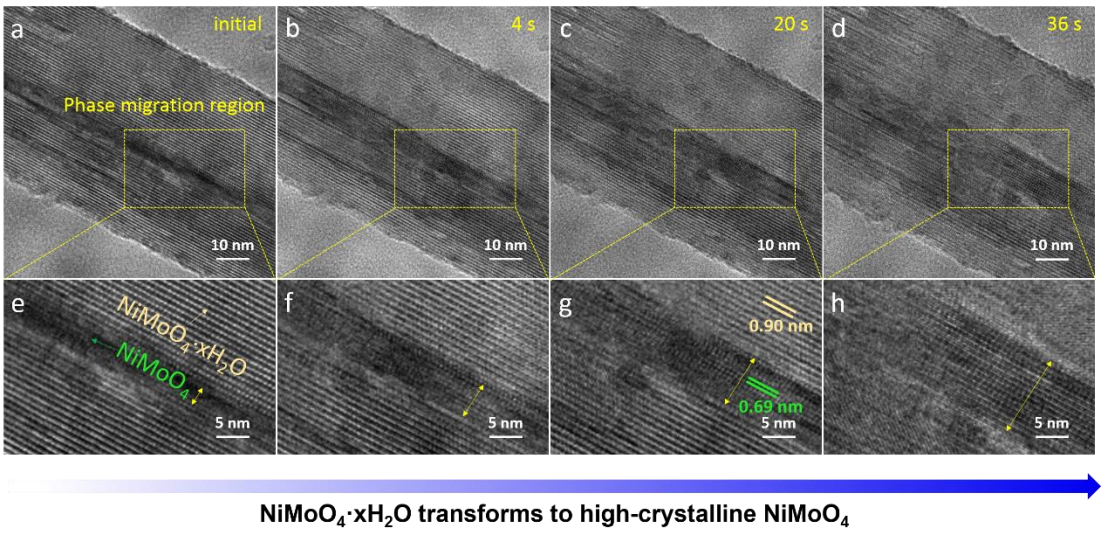

Figure S6. The *in-situ* TEM snapshots for the transformation processes of $NiMoO_4 \cdot xH_2O$ to $NiMoO_4$.

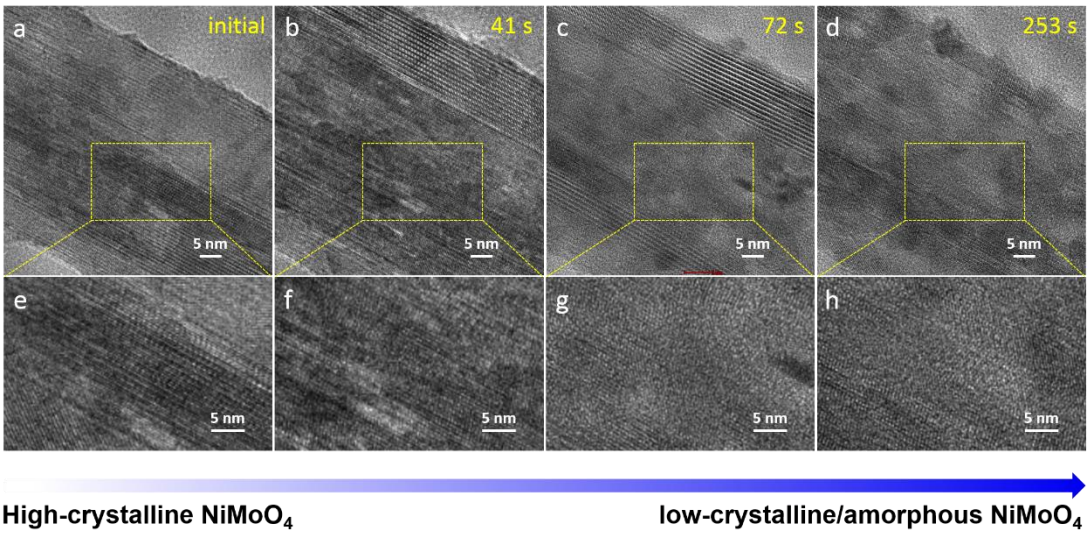

Figure S7. The *in-situ* TEM snapshots for the transformation from high-crystalline $NiMoO_4$ to low-crystalline/amorphous $NiMoO_4$.

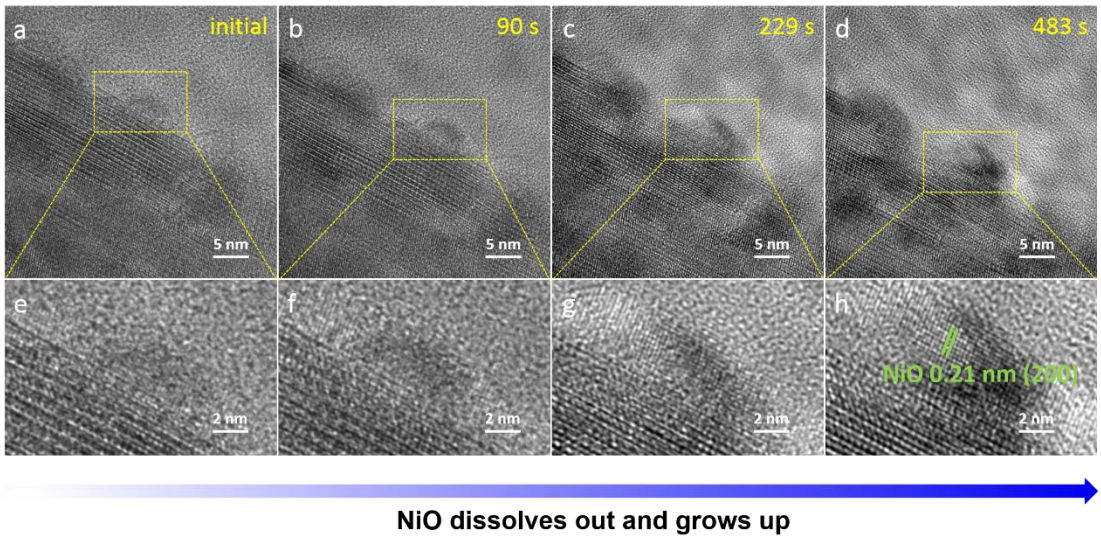

Figure S8. The *in-situ* TEM snapshots for the processes of NiO dissolution and growth.

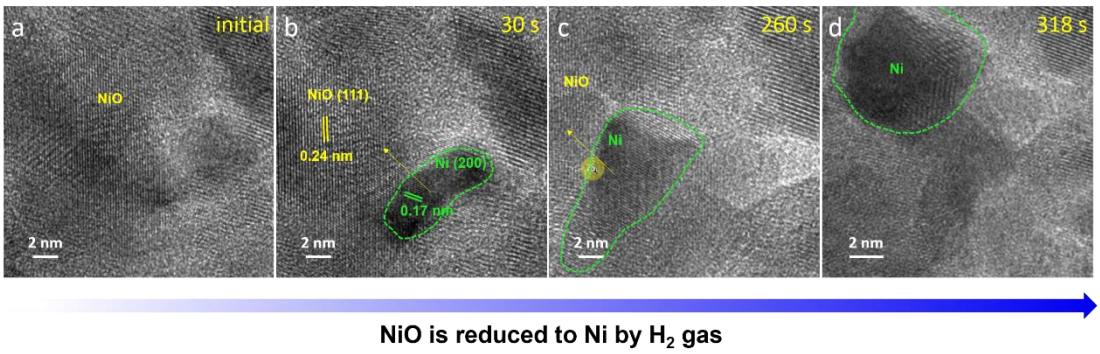

Figure S9. The *in-situ* TEM snapshots for the reduction processes of NiO to Ni.

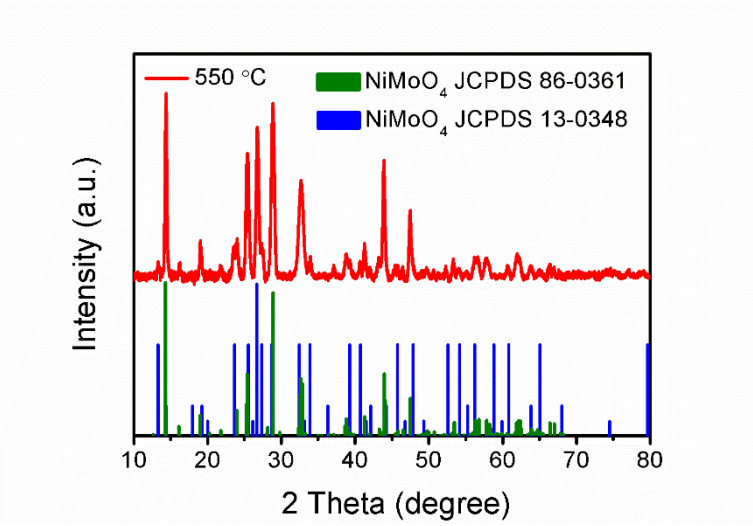

Figure S10. XRD pattern of the $NiMoO_4$ product derived from $NiMoO_4 \cdot xH_2O$, which is calcined at 550 °C in Ar.

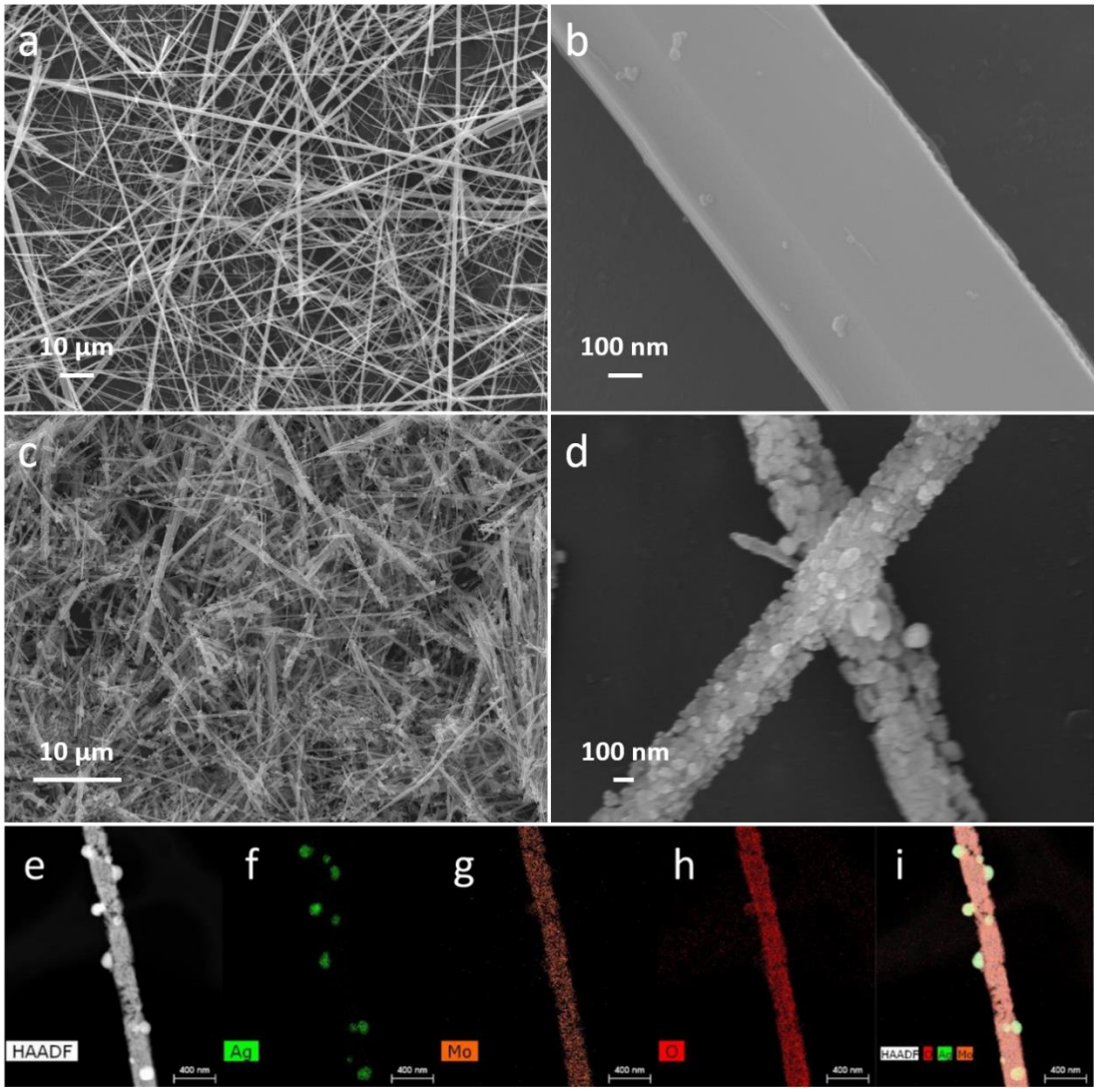

Figure S11. (a, b) SEM images of silver molybdate nanowires (Ag-Mo-O NWs). (c, d) SEM

images of MoO_2-Ag heterostructure nanowires. (e-i) HAADF-STEM images with elemental mappings for a single MoO_2-Ag nanowire.

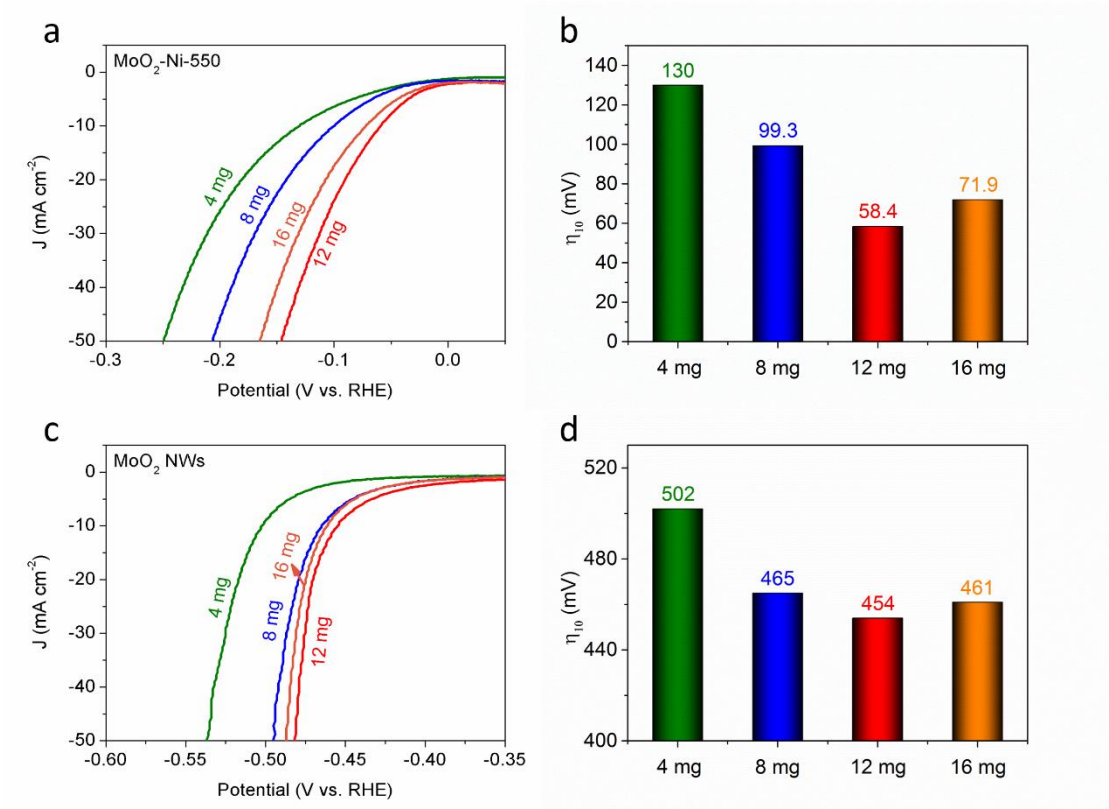

Figure S12. LSV curves and the corresponding η_{10} values of (a, b) MoO_2-Ni-550 and (c, d) MoO_2 NWs with the different mass loadings on glassy carbon, respectively.

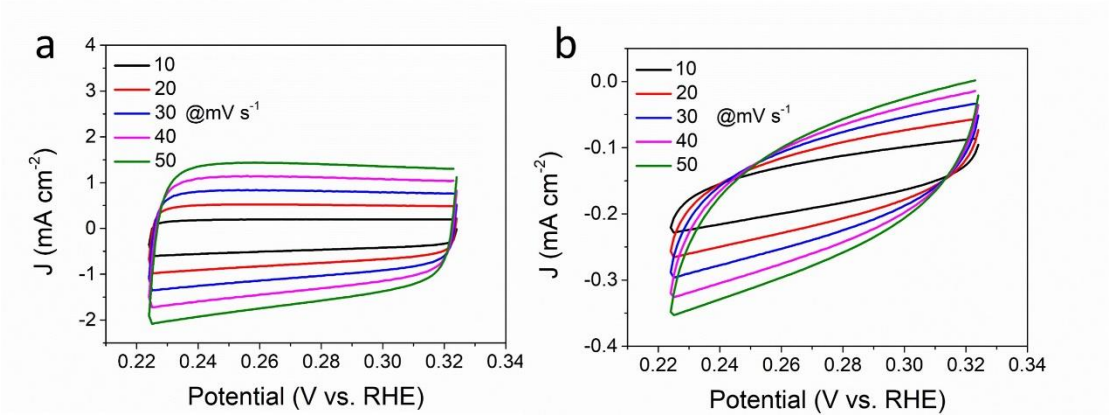

Figure S13. CV curves of (a) MoO_2-Ni NWs and (b) MoO_2 NWs at various scan rates. The current densities obtained at 0.274 V *vs.* RHE are used to calculate the C_{dl} values.

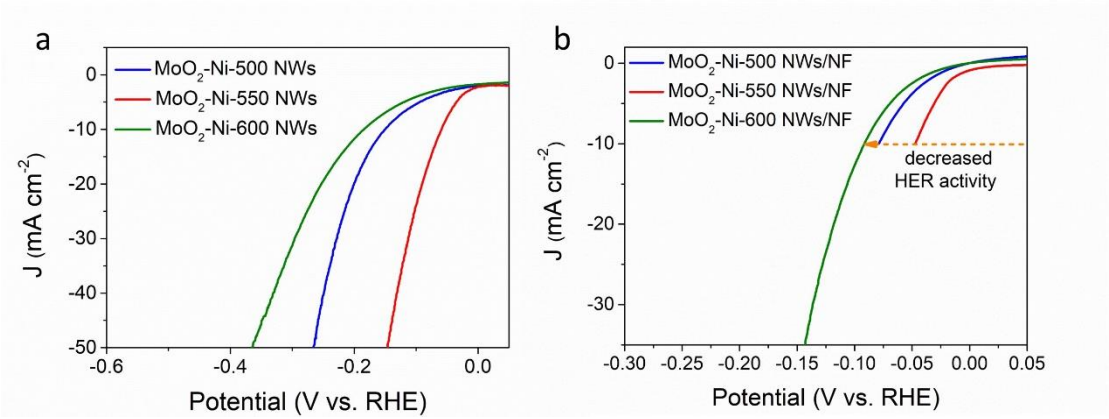

Figure S14. LSV curves of (a) MoO_2-Ni-x (x = 500, 550 and 600) NWs and (b) MoO_2-Ni-x (x = 500, 550 and 600) NWs/NF measured at 5 mV s^{-1} in 1 M KOH.

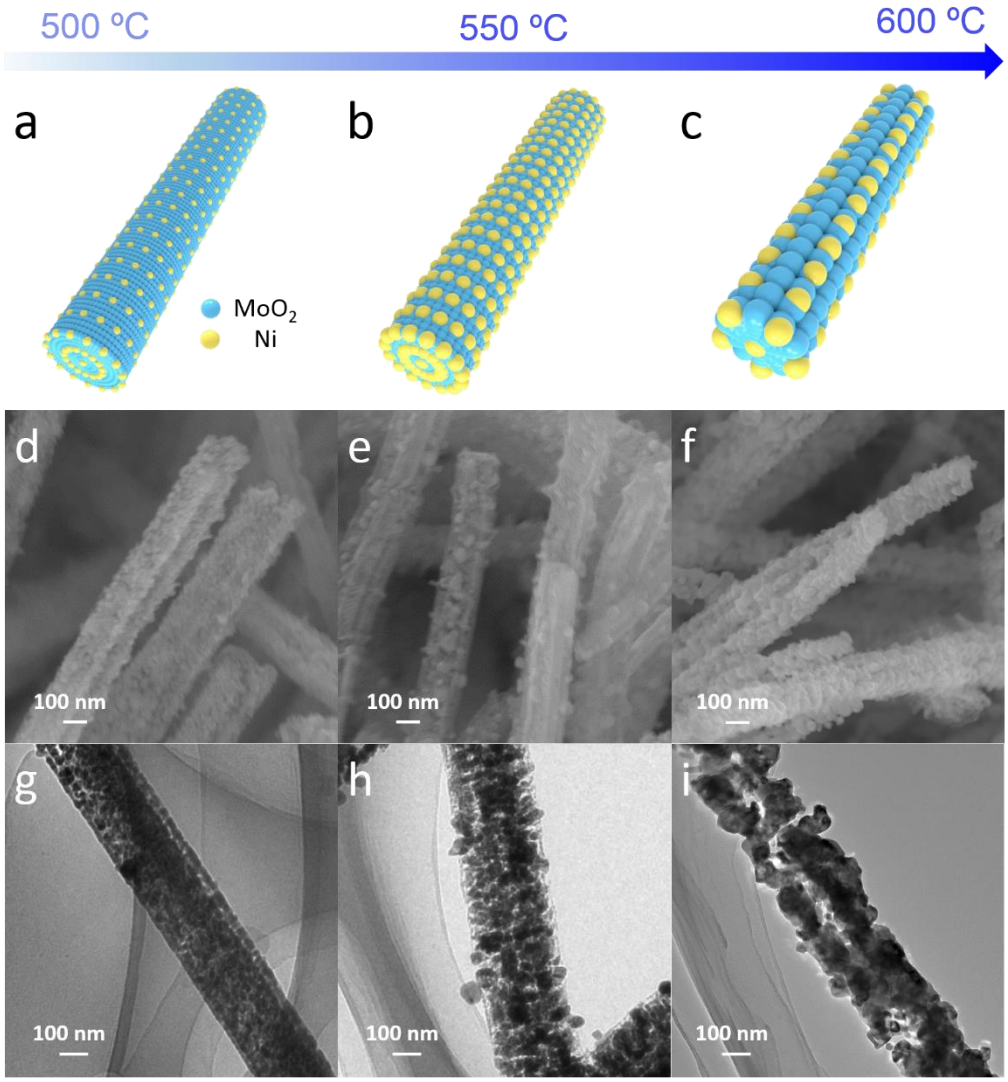

Figure S15. (a-c) Schematic illustration, (d-f) SEM and (g-h) TEM images of MoO_2-Ni-x (x = 500, 550 and 600), respectively.

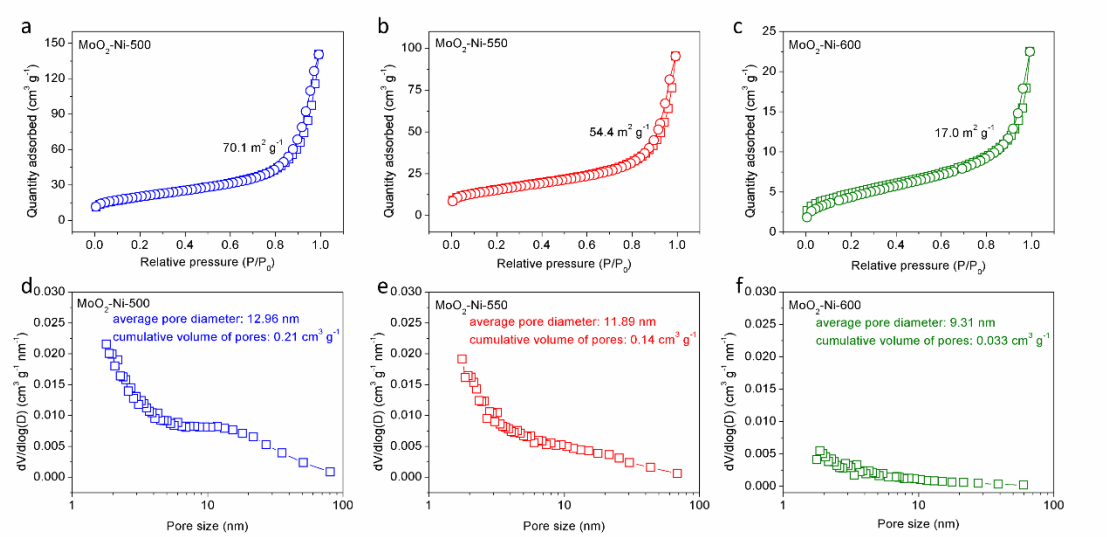

Figure S16. (a-c) Nitrogen absorption/desorption and (d-f) pore size distribution diagrams of MoO_2-Ni-x (x = 500, 550 and 600), respectively.

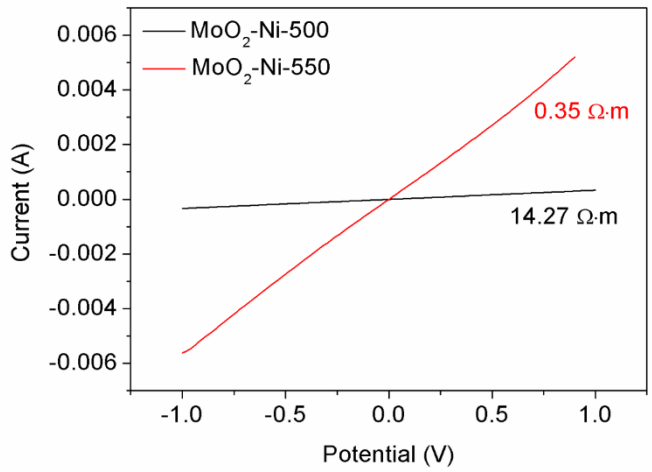

Figure S17. I-V curves of MoO_2-Ni-500 and MoO_2-Ni-550 powders by the Probe Station and Agilent B1500A Semiconductor Device Analyzer.

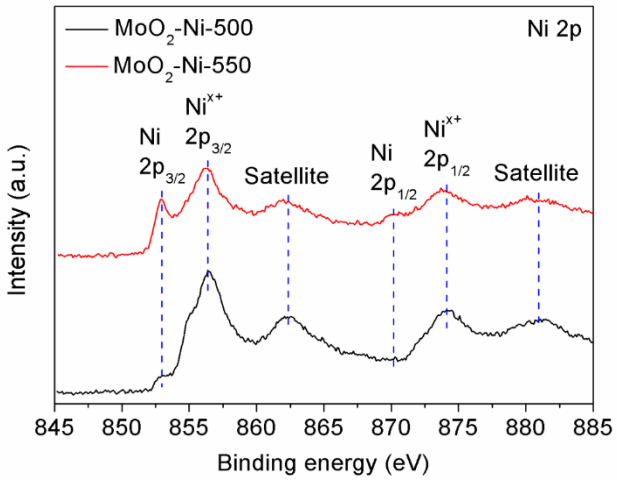

Figure S18. Ni 2p XPS spectra of MoO_2-Ni-500 and MoO_2-Ni-550.

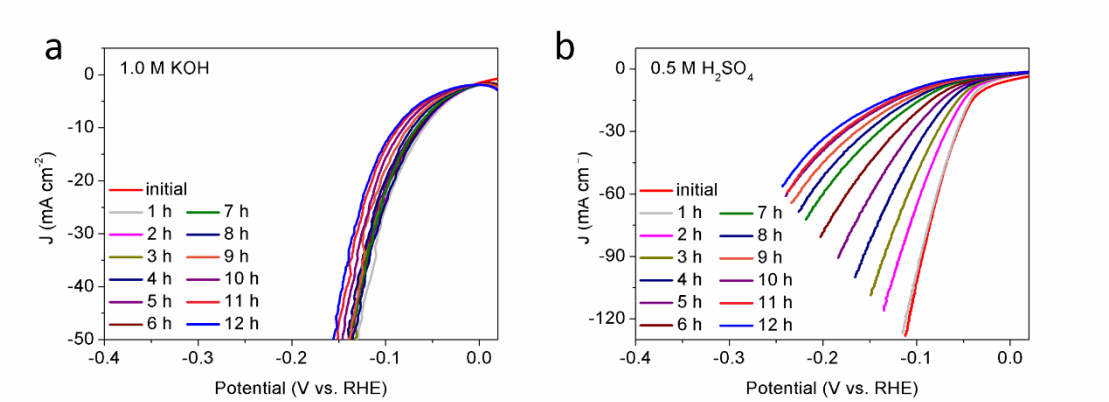

Figure S19. LSV curves of MoO_2-Ni NWs/NF after soaking in (a) 1 M KOH and (b) 0.5 M H_2SO_4 for different time, respectively.

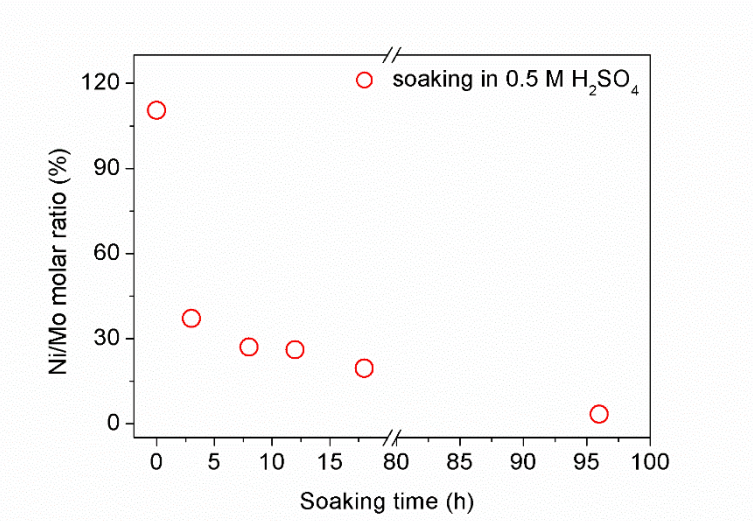

Figure S20. The Ni/Mo molar ratios of MoO_2-Ni-550 NWs after soaking in 0.5 M H_2SO_4 for different time, which were obtained by ICP measurement.

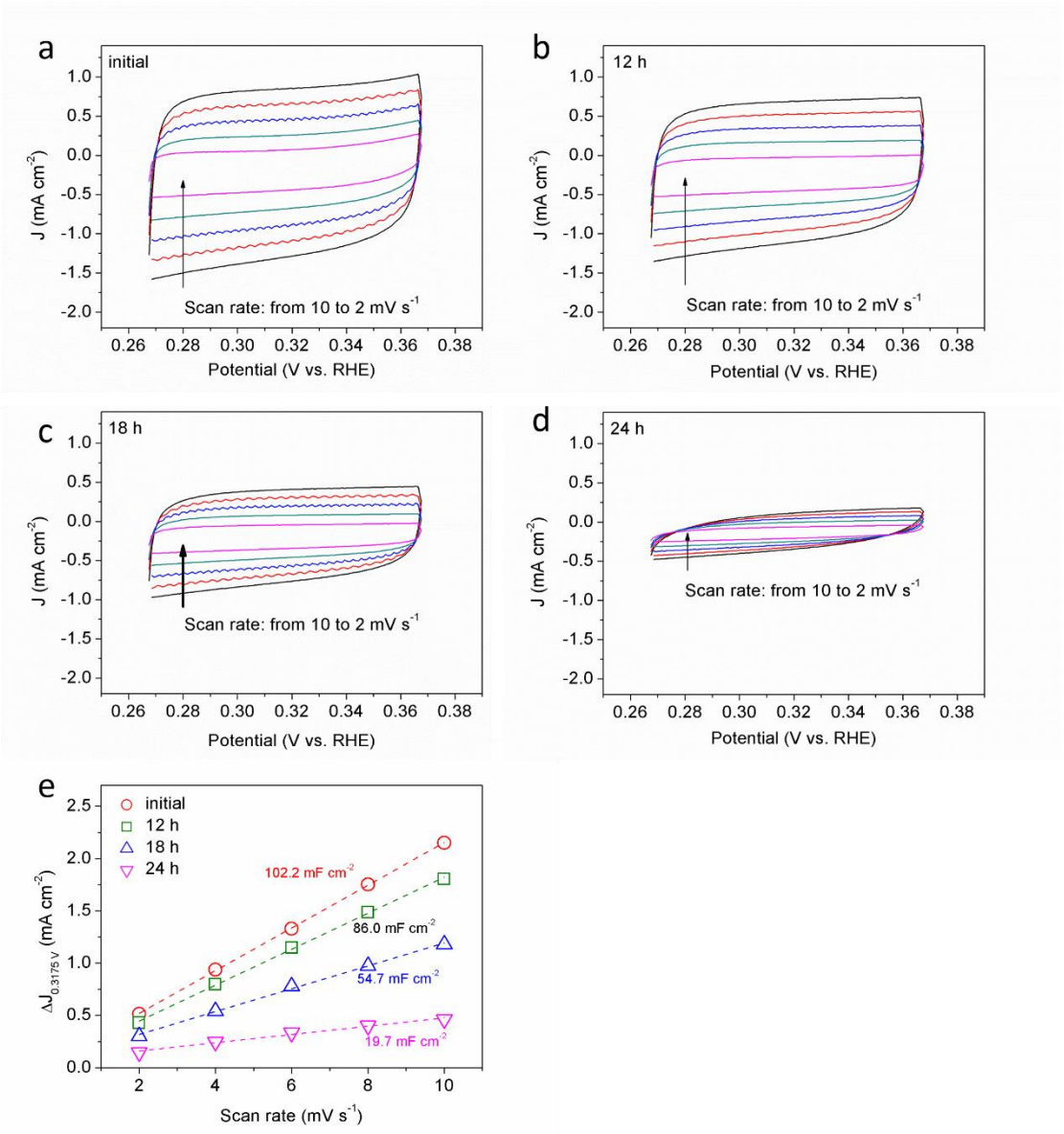

Figure S21. CV curves of MoO_2-Ni-550 NWs/NF after soaking in 0.5 M H_2SO_4 for (a) 0 h, (b) 12 h, (c) 18 h and (d) 24 h, respectively, which are measured in 1 M KOH at different scan rates. (e) The corresponding C_{dl} values obtained at 0.3175 V vs. RHE.

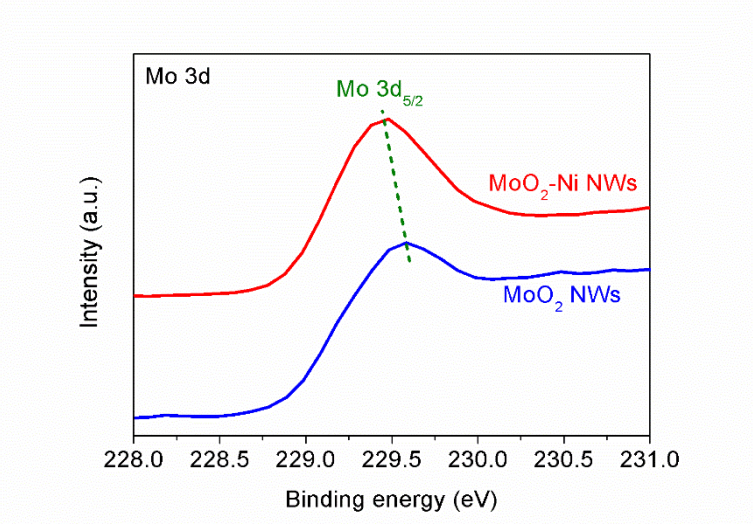

Figure S22. Mo 3d XPS spectra of MoO_2-Ni-550 NWs and MoO_2 NWs.

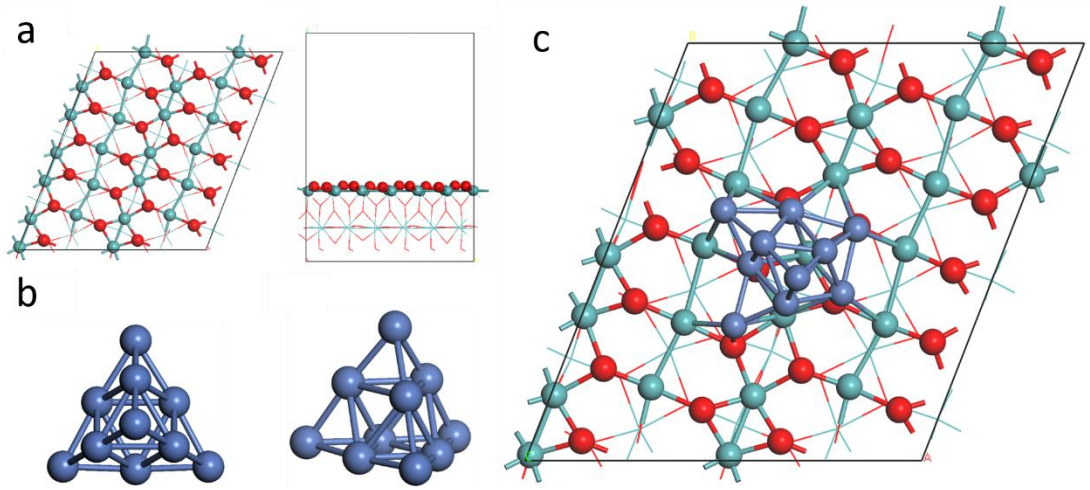

Figure S23. Optimized structure models for (a) MoO_2, (b) Ni and (c) MoO_2-Ni.

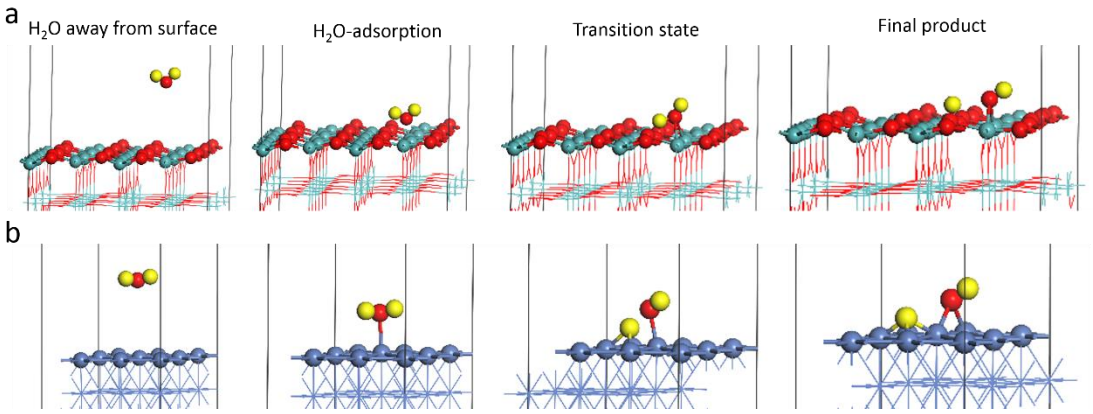

Figure S24. Optimized structure models for (a) MoO_2 and (b) Ni with four water-dissociation steps.

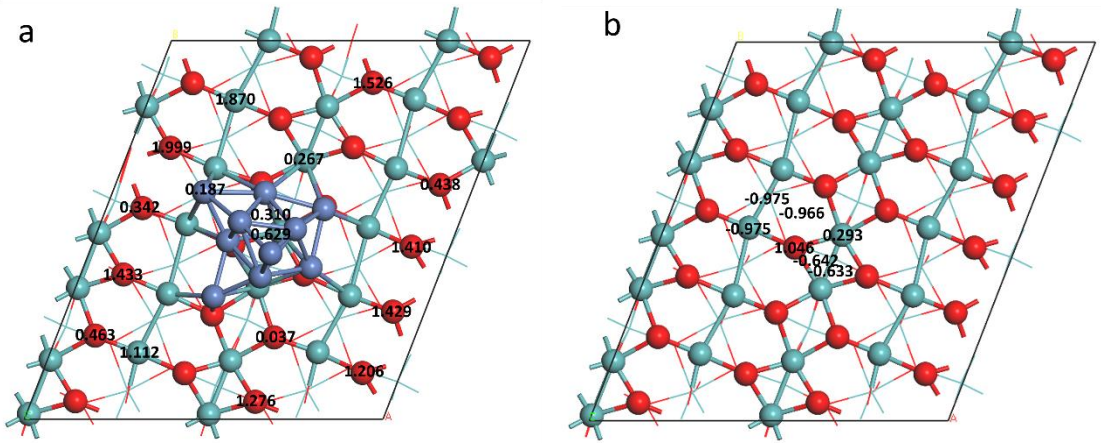

Figure S25. The ΔG_{H^*} values of hydrogen adsorption on the different sites for (a) MoO_2-Ni and (b) MoO_2 models.

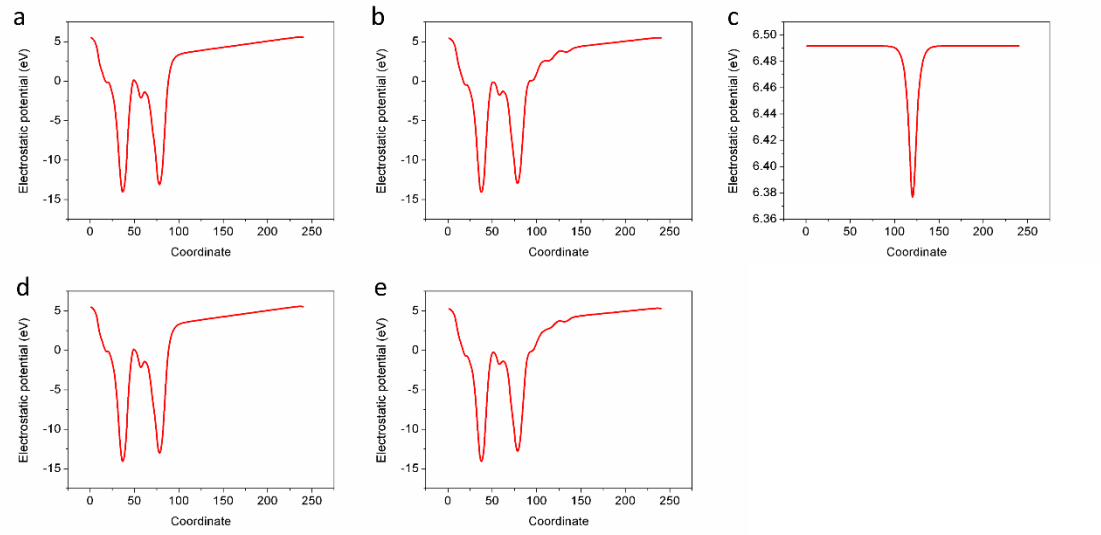

Figure S26. The calculated work function for (a) MoO_2, (b) MoO_2-Ni, (c) H atom, (d) H-adsorbed MoO_2 and (e) H-adsorbed MoO_2-Ni models.

To obtain the schematic diagram in **Figure 6b**, the following calculation formula for each models was adopted.

The x-axis values of PDOS data (taking the vacuum energy level as zero) = the x-axis values of PDOS data (taking the Fermi level as zero) - the calculated work function.

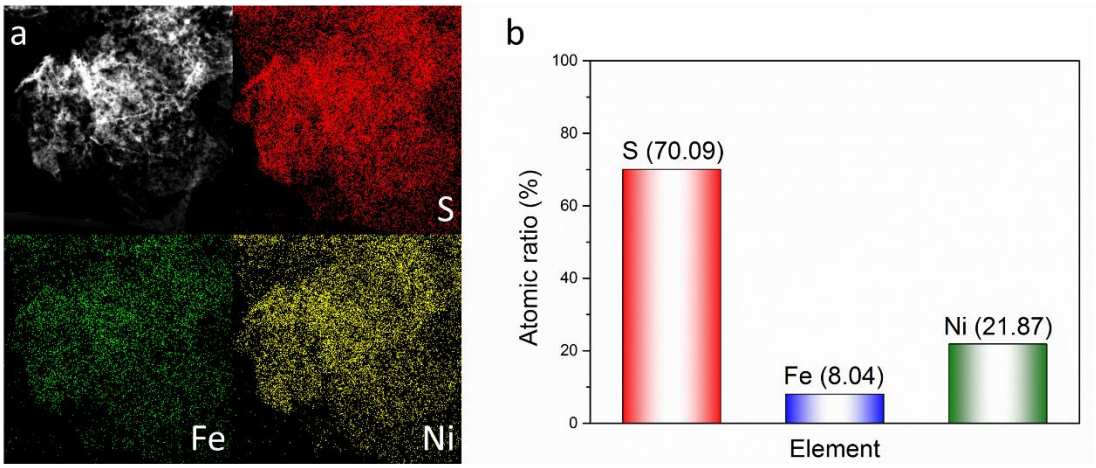

Figure S27. (a) HAADF-STEM images with elemental mappings of NiFe-S nanosheets. (b) EDX results of atomic ratios in NiFe-S nanosheets.

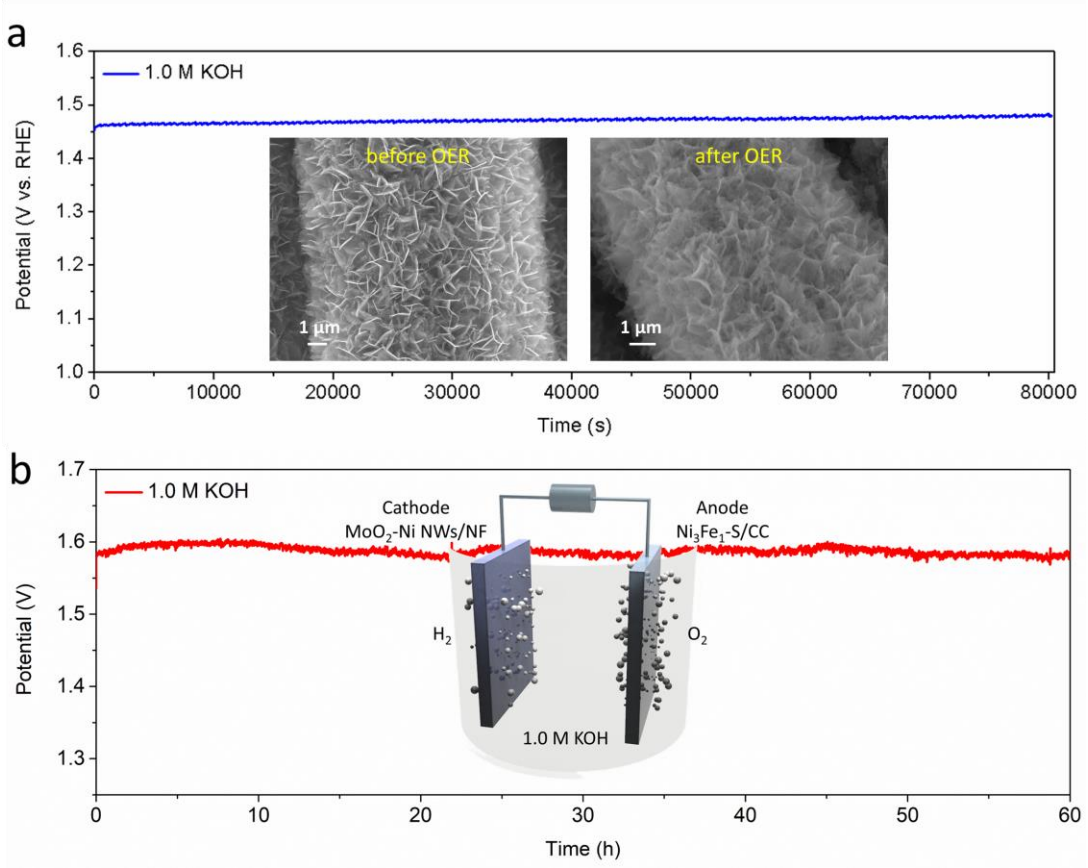

Figure S28. (a) Chronopotentiometric measurement of NiFe-S/CC at -10 mA cm^{-2} in 1 M KOH. The insets are the SEM images for NiFe-S/CC before and after stability test. (b) Performance of the electrolyzer held at 10 mA cm^{-2}. The inset is the schematic of electrolyzer, which uses MoO_2-Ni NWs/NF cathode and NiFe-S/CC anode in 1 M KOH.

Table S1. Summary of HER properties in 1 M KOH on our MoO_2-Ni NWs catalyst and the reported metal oxide-oxide catalysts.

Catalysts	η_{10} (mV)	References
MoO_2-Ni-550 NWs/NF	47	This work
MoO_2-Ni-550 NWs	58.4	
Co-Co_3O_4 NSs/NF[1]	~ 90	*Nano Lett.* **2015**, *15*, 6015-6021
Ni-CeO_2/CNTs[2]	91	*Nano Lett.* **2015**, *15*, 7704-7710
NiO-Ni/CNTs[3]	80	*Nat. Commun.* **2014**, *5*, 4695
Ni-MoO_2/CC[4]	40	*J. Mater. Chem. A* **2017**, *5*, 24453-24461
Co@CoO/NG[5]	72	*J. Mater. Chem. A* **2016**, *4*, 12046-12053
Co/CoO/Co_3O_4@NC[6]	232	*J. Am. Chem. Soc.* **2015**, *137*, 2688-2694
Ni-NiO/NG/NF[7]	140	*Adv. Funct. Mater.* **2015**, *25*, 5799-5808
Co-CoO/NG/NF[7]	170	
Ni/NiO NSs[8]	145	*J. Power Sources* **2015**, *300*, 336-343

Table S2. Comparison of the cell voltages at 10 mA cm^{-2} (V_{10}) of our assembled water-splitting device with currently available robust water-splitting device in 1 M KOH.

Cathode and anode catalysts	V_{10} (V)	References
MoO_2-Ni-550 NWs/NF and NiFe-S/CC	~ 1.58	This work
CoNi@NC-600 and CoNi@NC-600[9]	~ 1.67	*Nano Lett.* **2017**, *17*, 7773-7781
BP/Co_2P and BP/Co_2P[10]	1.92	*Angew. Chem. Int. Ed.* **2018**, *57*, 2600-2604
$NiMoO_{4-x}$/MoO_2 and $NiMoO_{4-x}$/MoO_2[11]	1.56	*J. Mater. Chem. A* **2018**, *6*, 12361-12369
Ni-Co-P and Ni-Co-P[12]	1.62	*Energy Environ. Sci.* 2018, 11, 872-880
Ni_3S_2/NF and Ni_3S_2/NF[13]	~ 1.76	*J. Am. Chem. Soc.* **2015**, *137*, 14023-14026
Co@NC/NF and Co@NC/NF[14]	1.59	*Adv. Energy Mater.* **2018**, *8*, 1702838
VOOH and VOOH[15]	1.62	*Angew. Chem. Int. Ed.* **2016**, *129*, 588-592
$NiCo_2O_4$ and $NiCo_2O_4$[16]	1.65	*Angew. Chem. Int. Ed.* **2016**, *128*, 6398-6402
$NiFeO_x$/CFP and $NiFeO_x$/CFP[17]	1.55	*Nat. Commun.* **2015**, *6*, 7261

References

(1) Yan, X. D.; Tian, L. H.; He, M.; Chen, X. B. Three-Dimensional Crystalline/Amorphous Co/Co_3O_4 Core/Shell Nanosheets as Efficient Electrocatalysts for the Hydrogen Evolution Reaction. *Nano Lett.* **2015**, *15*, 6015-6021.

(2) Weng, Z.; Liu, W.; Yin, L. -C.; Fang, R. P.; Li, M.; Altman, E. I.; Fan, Q.; Li, F.; Cheng, H. M.; Wang, H. L. Metal/Oxide Interface Nanostructures Generated by Surface Segregation For Electrocatalysis. *Nano Lett.* **2015**, *15*, 7704-7710.

(3) Gong, M.; Zhou, W.; Tsai, M. C.; Zhou, J. G.; Guan, M. Y.; Lin, M. C.; Zhang, B.; Hu, Y. F.; Wang, D. Y.; Yang, J.; Pennycook, S. J.; Hwang, B. J.; Dai, H. J. Nanoscale Nickel Oxide/Nickel Heterostructures for Active Hydrogen Evolution Electrocatalysis. *Nat. Commun.* **2014**, *5*, 4695.

(4) Ren, B. W.; Li, D. Q.; Jin, Q. Y.; Cui, H.; Wang, C. X. Integrated 3D Self-Supported Ni Decorated MoO_2 Nanowires as Highly Efficient Electrocatalysts for Ultra-Highly Stable and Large-Current-Density Hydrogen Evolution. *J. Mater. Chem. A* **2017**, *5*, 24453-24461.

(5) Zhang, S.; Yu, X. B.; Yan, F.; Li, C. Y.; Zhang, X. T.; Chen, Y. J. N-Doped Graphene-Supported Co@CoO Core-Shell Nanoparticles as High-Performance Bifunctional Electrocatalysts for Overall Water Splitting. *J. Mater. Chem. A* **2016**, *4*, 12046-12053.

(6) Jin, H. Y.; Wang, J.; Su, D. F.; Wei, Z. Z.; Pang, Z. F.; Wang, Y. In Situ Cobalt-Cobalt Oxide/N-Doped Carbon Hybrids as Superior Bifunctional Electrocatalysts for Hydrogen and Oxygen Evolution. *J. Am. Chem. Soc.* **2015**, *137*, 2688-2694.

(7) Liu, X. E.; Liu, W.; Ko, M.; Park, M.; Kim, M. G.; Oh, P.; Chae, S.; Park, S.; Casimir, A.; Wu, G.; Cho, J. Metal (Ni, Co)-Metal Oxides/Graphene Nanocomposites as Multifunctional Electrocatalysts. *Adv. Funct. Mater.* **2015**, *25*, 5799-5808.

(8) Yan, X. D.; Tian, L. H.; Chen, X. B. Crystalline/Amorphous Ni/NiO Core/Shell Nanosheets as Highly Active Electrocatalysts for Hydrogen Evolution Reaction. *J. Power Sources* **2015**, *300*, 336-343.

(9) Meng, J. S.; Liu, X.; Li, J. T.; Li, Q.; Zhao, C.; Xu, L. H.; Wang, X. P.; Liu, F.; Yang, W.; Xu, X. M.; Liu, Z. A.; Niu, C. J.; Mai, L. Q. General Oriented Synthesis of Precise Carbon-Confined Nanostructures by Low-Pressure Vapor Superassembly and Controlled Pyrolysis. *Nano Lett.* **2017**, 17, 7773-7781.

(10) Wang, J. H.; Liu, D. N.; Huang, H.; Yang, N.; Yu, B.; Wen, M.; Wang, X.; Chu, P. K.; Yu, X. F. In-Plane Black Phosphorus/Dicobalt Phosphide Heterostructure for Efficient Electrocatalysis. *Angew. Chem. Int. Ed.* **2018**, *57*, 2600-2604.

(11) Zheng, Z.; Ma, X. X.; Tang, J. L. Porous $NiMoO_{4-x}/MoO_2$ Hybrids as Highly Effective Electrocatalysts for the Water Splitting Reaction. *J. Mater. Chem. A* **2018**, *6*, 12361-12369.

(12) Hu, E. L.; Feng, Y. F.; Nai, J. W.; Zhao, D.; Hu, Y.; Lou, X. W. Construction of Hierarchical Ni-Co-P Hollow Nanobricks with Oriented Nanosheets for Efficient Overall Water Splitting. *Energy Environ. Sci.* **2018**, *11*, 872-880.

(13) Feng, L. L.; Yu, G. T.; Wu, Y. Y.; Li, G. D.; Li, H.; Sun, Y. H.; Asefa, T.; Chen, W.; Zou, X. X.

High-Index Faceted Ni_3S_2 Nanosheet Arrays as Highly Active and Ultrastable Electrocatalysts for Water Splitting. *J. Am. Chem. Soc.* **2015**, *137*, 14023-14026.

(14) Sivanantham, A.; Ganesan, P.; Estevez, L.; McGrail, B. P.; Motkuri, R. K.; Shanmugam, S. A Stable Graphitic, Nanocarbon-Encapsulated, Cobalt-Rich Core-Shell Electrocatalyst as an Oxygen Electrode in a Water Electrolyzer. *Adv. Energy Mater.* **2018**, *8*, 1702838.

(15) Shi, H, H.; Liang, H. F.; Ming, F. W.; Wang, Z. C. Efficient Overall Water-Splitting Electrocatalysis Using Lepidocrocite VOOH Hollow Nanospheres. *Angew. Chem. Int. Ed.* **2016**, *129*, 588-592.

(16) Gao, X. H.; Zhang, H. X.; Li, Q. G.; Yu, X. G.; Hong, Z. L.; Zhang, X. W.; Liang, C. D.; Lin, Z. Hierarchical $NiCo_2O_4$ Hollow Microcuboids as Bifunctional Electrocatalysts for Overall Water-Splitting. *Angew. Chem. Int. Ed.* **2016**, *128*, 6398-6402.

(17) Wang, H. T.; Lee, H. W.; Deng, Y.; Lu, Z. Y.; Hsu, P. C.; Liu, Y. Y.; Lin, D. C.; Cui, Y. Bifunctional Non-Noble Metal Oxide Nanoparticle Electrocatalysts through Lithium-Induced Conversion for Overall Water Splitting. *Nat. Commun.* **2015**, *6*, 7261.